Applied Catalysis B: Environmental 181 (2016) 848–861

Contents lists available at ScienceDirect

Applied Catalysis B: Environmental

journal homepage: www.elsevier.com/locate/apcatb

Low temperature catalytic combustion of 1,2-dichlorobenzene over CeO_2–TiO_2 mixed oxide catalysts

Wei Deng, Qiguang Dai*, Yijie Lao, Bingbing Shi, Xingyi Wang*

Lab for Advanced Materials, Research Institute of Industrial Catalysis, East China University of Science and Technology, Shanghai 200237, PR China

ARTICLE INFO

Article history:
Received 25 April 2015
Received in revised form 28 July 2015
Accepted 29 July 2015
Available online 31 July 2015

Keywords:
1,2-Dichlorobenzene
Catalytic combustion
Ceria
Titania

ABSTRACT

$Ce_{1-x}Ti_xO_2$ mixed oxide catalysts with various Ti/Ce + Ti ratios were prepared by sol–gel way and used in catalytic combustion of 1,2-dichlorobenzene (*o*-DCB). Characterization by XRD, Raman, HRTEM, XPS, H_2-TPR, O_2-TPD, CO_2-TPD and NH_3-TPD revealed that $Ce_{1-x}Ti_xO_2$ catalysts were identified as the forms of fluorite, monocline and anatase. The incorporation of Ti distorted the crystal structure and thus increased greatly the acidity and the oxygen mobility at high temperature. $Ce_{1-x}Ti_xO_2$ catalysts had considerable activity for *o*-DCB combustion. TOF obtained on the catalyst with Ti/Ce + Ti ratio of 0.1 at 275 °C reached the highest value of 0.64 μmol/min m^2 (Ti). Ti improved the stability of $Ce_{1-x}Ti_xO_2$ catalysts through retarding the exchange of Cl for basic lattice oxygen and hydroxyl groups. High stability maintained at 330 °C for at least 50 h. In situ FTIR indicated that *o*-DCB adsorption was much stronger on Ti species than Ce species and different reaction pathways were related to different types of oxygen species existing on the surface of $Ce_{1-x}Ti_xO_2$ catalysts.

1. Introduction

Chlorinated volatile organic compounds (CVOCs) in waste gases are released to the atmosphere from a wide range of industrial processes or the incineration of municipal and medical wastes. Among them, polychlorinated dibenzopdioxins (PCDDs) and poly chloro dibenzo furans (PCDFs) known as dioxins are chlorinated organic molecules belonging to the category of persistent organic pollutants (POPs) with high toxicity and carcinogenicity, able to persist in the ecosystem for several years [1]. Hence, stringent environmental regulations are in place in several countries limiting PCDD/PCDF emissions [2,3]. Therefore, various control methods have been designed and used [2,4], of which, catalytic oxidation is a preferred approach [3,5,6]. Its major advantage is that oxidation can be effectively performed at temperatures between 250 and 550 °C and very dilute pollutants which cannot be thermally combusted without additional fuel can be treated effectively by this way [7]. Another advantage is its excellent selectivity toward formation of the desired products such as carbon dioxide, HCl and water. Normally, considering PCDD/PCDFs' high toxicity and delicate manipulation in laboratories, model compounds have been used to evaluate the activity of the catalysts in the majority of these studies. Chlorobenzene (CB) and 1,2-dichlorobenzene (*o*-DCB) have been most frequently used, because of their structural similarity to PCDDs.

During the past decades, a number of catalyst systems for the total oxidation of chlorinated compounds were reported. Most of them were focused on three types of catalysts based on noble metals [3,6,7], transition metals [5,8,9] and zeolites [10–12]. The activity of noble metal catalysts was often very high, but they were susceptible to the deactivation by chlorine adsorption, and were also sensitive to higher temperatures. The activity of zeolites was related to their acid properties. However, the formation of polychlorinated compounds and the deposition of coke on these acidic catalysts are yet to be solved out. Transition metal oxides, in general, were less active than noble metals, but they can resist deactivation by chlorine adsorption to a larger extent [13]. And the use of transition metal catalysts can lower the cost because most of them are less expensive. Thus, there are few reports about transition metal oxides used for catalytic combustion of *o*-DCB in recent years, including V_2O_5/TiO_2 [2,4], $CaCO_3/-Fe_2O_3$ [14], $Fe–Ca–O_x/TiO_2$ [8], TiO_2-masked Fe_3O_4 [15], Mn-modified Co_3O_4 [16] and so on. V_2O_5/TiO_2 prepared by a sol–gel method showed a very high activity and stability for gas phase oxidation of *o*-DCB, but V_2O_5 was toxic so as to cause secondary pollution. $CaCO_3/-Fe_2O_3$ was an effective catalyst in *o*-DCB combustion, but the activity easily lost in the presence of water. So, development of catalysts having high catalytic performance and resistance to chlorine poisoning is of great interest.

* Corresponding authors. Fax: +86 21 64253372.
E-mail addresses: daiqg@ecust.edu.cn (Q. Dai), wangxy@ecust.edu.cn (X. Wang).

http://dx.doi.org/10.1016/j.apcatb.2015.07.053
0926-3373/

Ceria has been widely used as heterogeneous catalysts. The redox properties of ceria and the high lability of its lattice oxygen are among the most important factors that contribute to the catalytic reactivity of CeO_2 in oxidation reactions, in particular, for total oxidation reactions. Our previous work indicated that high activity for CB catalytic combustion of CeO_2-based catalysts mainly owed to the unique redox properties and high dissociation of C—Cl of CeO_2 [7,17,18] . However, the stability of CeO_2 can be achieved only at high temperature because of strong adsorption of inorganic chlorine species produced during the decomposition of CB on the active sites [7,17,18]. The modification of CeO_2- based catalysts with transition metal oxides that promote the stable activity at lower temperature is still a challenge. To our best knowledge, V_2O_5/TiO_2 was found to be suitable for the chemical resistance to chlorine-poisoning [19–21]. And RuO_2/TiO_2 has been identified as an efficient catalyst for HCl oxidation (Deacon reaction) in the temperature range of 250–350 °C [22]. It is expected that introduction of TiO_2 could improve the ability of CeO_2 resistance to chlorine-poisoning. However, few studies on the behaviors of $Ce_{1-x}Ti_xO_2$ mixed oxide catalysts in the oxidation of CVOCs were available. In this study, $Ce_{1-x}Ti_xO_2$ catalysts with various Ti/Ce + Ti ratios were prepared by sol-gel method and investigated in *o*-DCB catalytic combustion by in situ FTIR and information on kinetics was concluded.

2. Experimental

2.1. Catalysts preparation

$Ce_{1-x}Ti_xO_2$ mixed oxide catalysts were prepared by a sol-gel method. $Ce(NO_3)_3$ ethanol solution was added to $Ti[O(CH_2)_3CH_3]_4$ ethanol solution with a given ratio of Ti/Ti + Ce under stirring. The solution was slowly gelled after finishing the reaction between $Ti[O(CH_2)_3CH_3]_4$ and H_2O at 40 °C. The gel was dried at 110 °C overnight and then calcined at 500 °C for 4 h. CeO_2 and TiO_2 were synthesized with the same method. The obtained $Ce_{1-x}Ti_xO_2$ samples with various ratios of Ti/Ce + Ti were denoted as $Ce_{1-x}Ti_x$ where *x* represents the atomic ratio of Ti/Ce + Ti.

2.2. Catalysts characterization

Characterization by XRD, Raman, TEM/HRTEM, XPS, H_2- TPR, O_2-TPD and CO_2-TPD was carried out by the methods as reported previously by our group and the details refer to Ref. [23]. The temperature programmed desorption of NH_3 (NH_3-TPD) was measured using a PX200A type TPD/TPR setup from Tianjin Pengxiang Tech. Corp.. Before measurement, each sample (100 mg) was heated under ultrapure He atmosphere at 30 ml/min at 500 °C for 1 h to remove surface adsorbates, cooled to 150 °C, saturated with 5% NH_3 in He and finally purged with He to remove physisorbed NH_3. The effluent of NH_3-TPD was quantified by TCD at a heating rate of 10 °C/min.

2.3. Catalytic activity measurement

Catalytic combustion reactions were carried out at atmospheric pressure in a continuous flow micro-reactor of a quartz tube of 4 mm inner diameter. 200 mg catalyst sample (grain size, 40–60 mesh) was packed in the reactor bed. Before testing the activity and selectivity of the prepared catalysts, the transport effects were investigated to ensure that experimental results were not significantly influenced by interphase transportation with the method previously reported [23]. For a typical *o*-DCB oxidation, the reactant feed was 1000 ppm *o*-DCB, 10% O_2 and N_2 balance. The temperature of reactor was measured with a thermocouple located just at the bottom of the micro-reactor and the effluent gases were analyzed on-line at a given temperature by using two gas chromatographs (GC), of which one was equipped with FID for the quantitative analysis of the organic chlorinated reactant. Catalytic activity was measured over the range 100–500 °C and the conversions were calculated by subtracting the outlet concentration from the inlet concentration of the reactant and dividing by the inlet concentration. These conversions were obtained at different temperatures under steady state at each temperature. All the reactions were repeated three times to assure reproducibility and rule out catalyst deactivation. More details about the determination of the activity and selectivity of catalysts in *o*-DCB oxidation refer to Ref. [16]. Furthermore, carbon balances could be as accurate as within 5% and only CO/CO_2 and trace 1,2,4-trichloro-benzene (TCB) were detected in the analyses of the products carbon-containing. The determination of reactants (*o*-DCB and oxygen) and products (CO/CO_2, HCl, Cl_2, benzene (B), CB and TCB) was carried out by the methods also previously reported [16].

2.4. In situ FTIR studies

FTIR spectra were collected with a Nicolet 740 spectrometer equipped with a MCT-B detector cooled by liquid nitrogen. A homemade flow cell with a path length of 10 cm, capped at both ends by IR-transparent NaCl windows, was used for in situ measurements. 100 mg sample was pressed into self-supported discs of approximately 1 cm diameter and placed in a sample holder at the center of the cell. The cell was heated externally and the temperature was measured by a thermocouple placed in close proximity to a catalyst. Transmission spectra were collected in the single-beam mode by recording 128 scans at a resolution of 4 cm^{-1}. Before each experiment, samples were pretreated in flowing 10% O_2/N_2 at 400 °C for 2 h. Spectra of the clean catalyst surface were collected and used as the background. Adsorption (or oxidation) studies were conducted by exposing samples to a stream of a flowing composed of 1000 ppm *o*-DCB and N_2 balance (or 10% O_2 and N_2 balance). In situ FTIR spectra were collected at different temperature where a steady state was reached.

3. Results and discussion

3.1. Sample characterization

Wide angle XRD patterns of $Ce_{1-x}Ti_xO_2$ samples with various Ti/Ti + Ce ratios (*R*) are shown in Fig. 1. The fcc fluorite structure

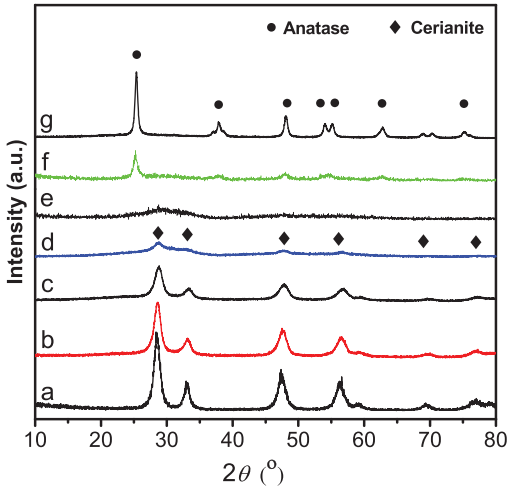

Fig. 1. XRD patterns of $Ce_{1-x}Ti_xO_2$ samples; a- CeO_2, b-$Ce_{0.9}Ti_{0.1}$, c-$Ce_{0.7}Ti_{0.3}$, d-$Ce_{0.5}Ti_{0.5}$, e-$Ce_{0.3}Ti_{0.7}$, f- $Ce_{0.1}Ti_{0.9}$ and g-TiO_2.

Table 1
Physical and chemical properties of $Ce_{1-x}Ti_xO_2$ samples.

Sample	Ce/Ce + Ti[a]	S_{BET}[b] (m^2/g)	P (nm)[c]	R(nm)[d]	L (nm)[e]		NH_3-TPD[f] (a.u.)			H_2 uptake (m mol/g)[g]		
							a	*b*	*c*	$Value_E$	$Value_T$[h]	V_E/V_{Total}[i]
CeO_2	1	76	11.1	12.0	0.5416		1.46	0.74	0	0.33	–	0.14
$Ce_{0.9}Ti_{0.1}$	0.8837	78	10.8	10.6	0.5372		1.19	1.66	0.31	0.40	0.32	0.16
$Ce_{0.7}Ti_{0.3}$	0.6774	80	9.3	10.0	0.5359		2.41	2.49	0.64	0.66	0.31	0.26
$Ce_{0.5}Ti_{0.5}$	0.4624	100	5.3	8.0	0.5390		3.10	4.62	1.48	0.96	0.30	0.51
$Ce_{0.3}Ti_{0.7}$	0.2857	154	3.8	–	–		7.12	4.29	2.40	0.47	0.32	0.42
$Ce_{0.1}Ti_{0.9}$	0.0826	79	5.3	16.1	*a* = 0.3832	*c* = 0.9097	3.12	4.86	1.46	0.16	0.06	0.41
TiO_2	0	20	–	18.2	*a* = 0.3777	*c* = 0.9421	0.65	1.72	0.51	0	–	–

[a] Ce/Ce + Ti ratios measured by XRF;
[b] BET surface area;
[c] BJH adsorption average pore diameter;l
[d] Crystalline size calculated from the Scherrer's equation, applied to the <111> reflection from cerianite;
[e] Lattice parameters;
[f] Values intergated under *a*, *b* and *c* peaks on profiles;
[g] H_2 uptake, according to TPR profile in a range of 200–650 °C;
[h] Theoretical values according to the assumption that H_2 consumption is resulted only from the reduction of Ce^{4+} into Ce^{3+} (Table S1);
[i] Theoretical total H_2 consumption of 1 g catalyst (Table S1).

of cerianite, with the diffraction peaks at 28.6, 33.0, 47.5, 56.3, 59.2, 69.3 and 76.7° (JCPDS No. 81–0792), is retained nearly down to *R* = 0.5, while the anatase structure of TiO_2 is formed nearly at *R* = 0.9. However, the intermediate compositions at *R* = 0.5–0.7 form mixed phases [24]. With the increase in *R*, a more asymmetric shape of such reflections from ceria fluorite with a lower intensity confirms the weakening degree of the crystallinity of samples, which is consistent with the increase in surface area (Table 1). Indeed, the fact that the average particle size of ceria, calculated from the peak at 28.6° of <1 1 1> crystal plane using Scherrer equation, is inversely proportional to surface area, which denotes main contribution of the matrix to surface area exposure. CeO_2 possesses surface area of 76 m^2/g, while $Ce_{1-x}Ti_xO_2$ samples exhibit the trend of increasing surface area with the increase in R from 0.1 to 0.5. Moreover, the diffraction peaks of cubic fluorite-like structure shift to slightly higher values of Bragg angles in a range of 28.7–29.0°, indicating that a part of Ti species enter into the fluorite lattice to form Ce—O—Ti solid solutions [24]. As reported in Reference [25], the ionic radius of Ti^{4+} (0.068 nm) is smaller than that of Ce^{4+} (0.094 nm), and incorporation of Ti^{4+} into the fluorite lattice results in the decrease in lattice parameters, which is justified by the results shown in Table 1.

TiO_2 and $Ce_{0.1}Ti_{0.9}$ show a typical XRD pattern of anatase with diffractions at 25.3, 37.0, 48.1 and 54.3° (JCPDS No. 40- 1290). Moreover, for $Ce_{0.1}Ti_{0.9}$, the increase of lattice parameter in the *a*-axis is observed with a decrease of that in *c*-axis (Table 1), which corresponds to the shortening of metal-oxygen bond, resulting from localization where the electron density of Ti cation shifts toward empty lattice site. A significant decrease in crystallite size is observed from 18.2 nm for TiO_2 to 16.1 nm for $Ti_{0.9}Ce_{0.1}$ with the increase in surface area from 20 to 79 m^2/g. $Ce_{0.3}Ti_{0.7}$ shows highly dispersed distort crystal structure with the highest area of 154 m^2/g. The bulk compositions of $Ce_{1-x}Ti_xO_2$ samples determined by XRF are close to the normal values (Table 1), indicating that all precursors can be effectively precipitated by sol–gel method. N_2 adsorption and desorption isotherms (Fig. S1) show that pore size distribution of CeO_2 is in a range of 5–55 nm calculated from the adsorption isotherm branch. With the incorporation of Ti, the average pore size becomes small (Table 1), and is 5.3 and 3.8 nm for $Ce_{0.5}Ti_{0.5}$ and $Ce_{0.3}Ti_{0.7}$, respectively. For $Ce_{0.1}Ti_{0.9}$, this value increases to 5.3 nm with a much broader pore size distribution, implying the occurrence of new structure (Fig. S1).

Fig. 2 shows the Raman spectra of $Ce_{1-x}Ti_xO_2$ samples. CeO_2 spectrum is dominated by the strong F_{2g} mode of fluorite phase at 460 cm^{-1}. TiO_2 spectrum shows bands at 141, 199, 396, 511 and 633 cm^{-1}, ascribed to anatase phase [24]. $Ce_{0.1}Ti_{0.9}$ presents a similar spectrum to TiO_2, but the bands become broad and weak. The enlarged spectra of $Ce_{0.3}Ti_{0.7}$ and $Ce_{0.5}Ti_{0.5}$ (Fig. S2) show that the former contains monoclinic phase (the corresponding bands appear at 332 and 569 cm^{-1}) [24], while the latter essentially presents fluorite phase of CeO_2. The ν_{F2g} band is dominated by oxygen lattice vibrations and sensitive to crystalline symmetry [26] . With the incorporation of Ti, the formation of weak longer bonds of Ce—O or Ti—O in cubic fluorite-like structure was observed previously by EXAFS and further confirmed by the first-principles calculations [25] . $Ce_{0.5}Ti_{0.5}$ shows a weak ν_{F2g} band, due to significant distortion of cubic fluorite structure. On XRD patterns of $Ce_{0.3}Ti_{0.7}$, no reflection from monoclinic phase is found, due to poor crystallization. These phenomena indicate that a strong interaction occurs between ceria and titania in the mixed material.

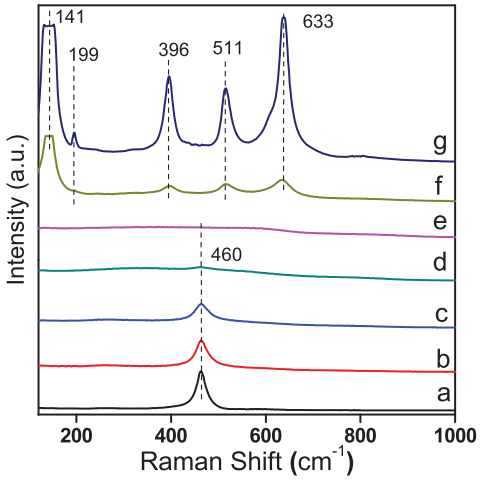

Fig. 2. Raman spectra of $Ce_{1-x}Ti_xO_2$ samples; a- CeO_2, b-$Ce_{0.9}Ti_{0.1}$, c-$Ce_{0.7}Ti_{0.3}$, d-$Ce_{0.5}Ti_{0.5}$, e-$Ce_{0.3}Ti_{0.7}$, f- $Ce_{0.1}Ti_{0.9}$ and g-TiO_2.

Fig. 3 shows HRTEM images of $Ce_{0.9}Ti_{0.1}$, $Ce_{0.5}Ti_{0.5}$ and $Ce_{0.1}Ti_{0.9}$. For $Ce_{0.9}Ti_{0.1}$ and $Ce_{0.5}Ti_{0.5}$, no evident difference in morphology is observed, while the size of observed CeO_2 particles of hexagon shape (white hexagons in Fig. 3A and B) decreases from 10 to 7 nm (Fig. S3A and S3B). Small CeO_2 particles stacked together to form a large plane. The lattice spacing is measured to be 0.31 nm, in good agreement with that of <1 1 1> crystal plane of the standard CeO_2 sample (JCPDS No.34-0394). The observation of electron diffraction rings in the selected area electron diffraction (SAED) patterns (insert of Fig. 3A and 3B) suggests the formation of a polycrystalline structure. Considerably small TiO_2 particles exposing <1 0 1> crys-

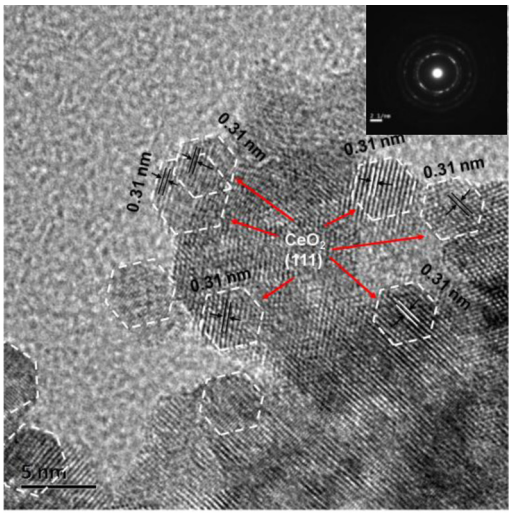

(A)

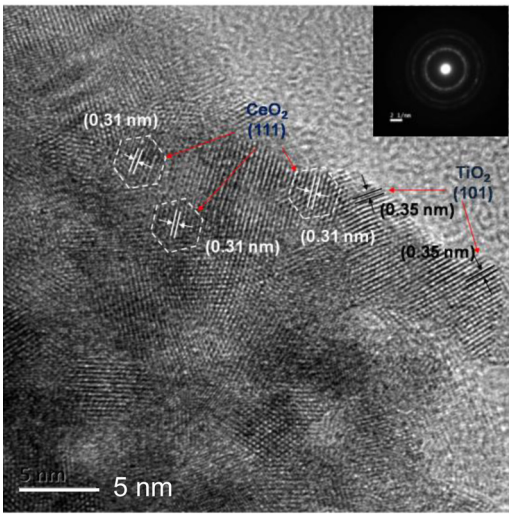

(B)

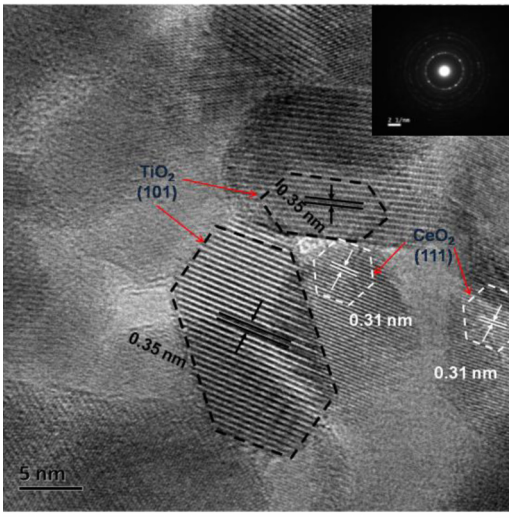

(C)

Fig. 3. HRTEM images and the selected area electron diffraction (SAED) patterns (insert) of $Ce_{0.9}Ti_{0.1}$ (A), $Ce_{0.5}Ti_{0.5}$ (B), $Ce_{0.1}Ti_{0.9}$ (C).

tal plane with lattice spacing of 0.35 nm (anatase, JCPDS No. 40-1290) along CeO_2 particles are observed only on $Ce_{0.5}Ti_{0.5}$, indicating that small content of Ti species for $Ce_{0.5}Ti_{0.5}$ can not incorporate into the fluorite structure. There is an upper limit for the incorporation of Ti species into the fluorite structure. As reported, the Ti limit content could be 40% [27]. On XRD pattern of $Ce_{0.5}Ti_{0.5}$, there appear no peaks relevant to diffraction peaks of TiO_2, owing to high dispersion of extra TiO_2 on the surface. Monocline structure is not found on $Ce_{0.5}Ti_{0.5}$, verifying that the band observed in a range of 192–364 cm^{-1} on Raman spectrum (Fig. S2B) could be not related to monoclinic structure. For $Ce_{0.1}Ti_{0.9}$, the particles with hexangle prismatic shape are ascribed to anatase TiO_2 (Fig. 3C and Fig. S3C). Moreover, small CeO_2 particles stacked together with anatase TiO_2 particles, indicating that there is also an upper limit for the incorporation of Ce^{4+} into TiO_2 lattice, probably being below 10%. The atomic maps (Fig. S4) obtained by EDS show that mixed oxides shows a good spatial dispersion of the two metals.

H_2-TPR measurement was used to investigate the reducibility of $Ce_{1-x}Ti_xO_2$ samples within 300–650 °C (Fig. 4A). For CeO_2, there appear two peaks, which are attributed to the reduction of Ce^{4+} to Ce^{3+} on the surface of nano- crystallites with different sizes [28]. With the incorporation of Ti, the peak intensity becomes strong and reaches the largest for $Ce_{0.5}Ti_{0.5}$ with disappearance of the peak at low temperature and the shift of peak temperature from 485 to 540 °C. H_2 consumption of $Ce_{1-x}Ti_xO_2$ samples is summarized in Table 1. According to the assumption that within 200–650 °C, H_2 consumption is ascribed only to $Ce^{4+} \rightarrow Ce^{3+}$, but not to $Ti^{4+} \rightarrow Ti^{3+}$, the calculated values (Table S1) are much lower than the experimental values. For the samples with $R = 0.5$ or lower, the reducibility of Ce^{4+} species increases from 14% for CeO_2 to 51% for $Ce_{0.5}Ti_{0.5}$, indicating that bulk lattice oxygen are abstracted by hydrogen. Here, the substitution of Ti for Ce can create a disorder which affects crystalline symmetry, resulting in the formation of weak long Ce—O and Ti—O bonds. As reported, for $Ce_{0.75}Ti_{0.25}O_2$, the oxygen sublattice was significantly distorted, leading to destabilization of oxide ions in terms of long Ce—O and Ti—O and short Ce—O and Ti—O bonds [25], where the oxide ions with longer bonds were weakly bound and the cohesive energy of $Ce_{0.75}Ti_{0.25}O_2$ was 15.5% smaller than that of CeO_2 [25]. For TiO_2-rich samples, the reducibility of Ce^{4+} species increases to 41% with the occurrence of initial reduction at somewhat high temperature.

O_2-TPD is an effective method to determine the mobility of oxygen species [29]. Generally, the adsorbed oxygen changes in the following procedures: O_2 (ad) → O_2^- (ad) → O (ad) → O^{2-} (lattice) [30]. The physically adsorbed oxygen O_2 and chemically adsorbed oxygen O_2^-/O^- species are much easier to desorb than the lattice O^{2-} species [31]. Oxygen desorption at very low temperature (<200 °C) can be assigned to the physically adsorbed oxygen and/or the ordinarily chemically adsorbed oxygen, while the desorption peaks between 200 and 400 °C can be related to the chemically adsorbed oxygen species, and the desorption peak appearing at higher temperatures (>400 °C) can be attributed to the lattice oxygen. As shown in Fig. 4B, for CeO_2, oxygen desorption starts at 266 °C and slowly becomes strong, indicating the presence of a small amount of chemically adsorbed oxygen species. However, oxygen desorption increases significantly at 400 °C or higher. Combining above H_2-TPR result that the reduction of bulk lattice oxygen can not occurs until 650 °C, it is reasonable that desorption at 400 °C or higher can be ascribed to surface lattice oxygen. With the presence of Ti, a distinctive feature is observed. For $Ce_{0.9}Ti_{0.1}$ and $Ce_{0.7}Ti_{0.3}$, chemically adsorbed oxygen species desorbed within 200–400 °C and the corresponding surface lattice oxygen desorbed at 436–469 °C decrease significantly, due to the decrease in CeO_2 clusters. However, surface lattice oxygen desorption shifts to low temperature (from 469 °C for CeO_2–436 °C for $Ce_{0.3}Ti_{0.7}$). Moreover, new strong peaks centered with maxima at 560–647 °C appear,

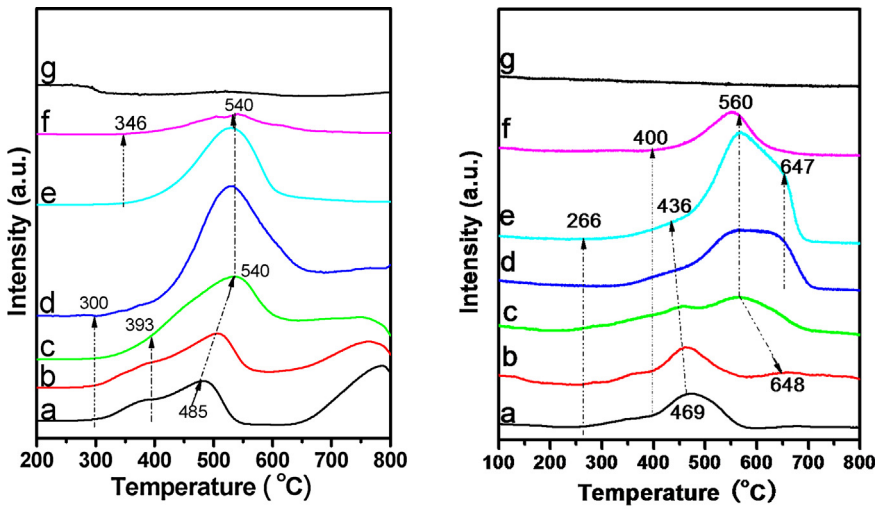

Fig. 4. H_2-TPR (A) and O_2-TPD (B) profiles of $Ce_{1-x}Ti_xO_2$ samples; a- CeO_2, b-$Ce_{0.9}Ti_{0.1}$, c-$Ce_{0.7}Ti_{0.3}$, d- $Ce_{0.5}Ti_{0.5}$, e-$Ce_{0.3}Ti_{0.7}$, f- $Ce_{0.1}Ti_{0.9}$ and g-TiO_2.

which can be ascribed to the desorption of bulk lattice oxygen species from weak Ce-O bonds due to the formation of $Ce_{1-x}Ti_xO_2$ solid solution. For $Ce_{0.1}Ti_{0.9}$, these oxygen species decrease due to too low Ce content. From H_2-TPR and O_2-TPD results, we can see that ceria-titania mixed oxide possess high oxygen storage capacity (OSC), while the weakly bound oxygen species should be responsible for higher OSC [25]. There is almost not any oxygen desorption observed on pure TiO_2.

Fig. 5 shows XPS spectra of Ce 3d, Ti 2p and O 1s electronic levels in $Ce_{1-x}Ti_xO_2$ samples. Typically, eight peaks resulting from the pairs of spin orbit doublets can be identified through deconvolution method, of which six peaks denoted as v, v'', v''', u, u'' and u''' arise from Ce^{4+} contributions while two peaks as v' and u', from Ce^{3+} contributions [32,33]. The proportion of Ce^{3+} ions with regard to the total cerium is calculated from the peak areas [34]. From the given results shown in Fig. 5A, the peaks of Ce^{3+} and Ce^{4+} ions are found with some changes in the intensity and position of peaks with the variation of Ti content. As reported, Ce^{3+} can be stabilized through the decrease in energy of Ce 4f levels as a result of the mixing with O 2p band of TiO_2 [35,36]. The reducibility of ceria does not diminish with the fraction of Ce^{3+} ions that are already present, because the additional electrons in Ce^{3+} occupy localized cerium f- states that do not interact with each other. For the samples with fluorite structure, the fraction of Ce^{3+} ions increases slowly due to the formation of a small amount of weak Ti—O—Ce (Table 2). For Ti-rich catalysts, the oxygen sub-lattice is significantly distorted, leading to destabilization of oxide ions in terms of long Ce—O and Ti—O and short Ce—O and Ti—O bonds; and Ce^{3+} ions increase greatly. Ti $2p_{3/2}$ peak shifts from 458.5 eV for TiO_2 to 457.7 eV for $Ce_{0.9}Ti_{0.1}$ (Fig. 5B), indicating that the oxidation state of Ti falls between trivalent and tetravalent [27]. Compared with the normal ratio of Ti/Ti + Ce, the enrichment of Ce on the surface is observed. With the increase in Ti content, the Ce+Ti/O ratio decreases significantly, probably due to the increase in Ce^{3+} or Ti $^{3+}$ species (Table 2).

XPS of O 1s for $Ce_{1-x}Ti_xO_2$ samples are deconvoluted into two contribution (Fig. 5C): one with binding energy of 528.9–530.0 eV is assigned to lattice oxygen (O_{latt}), and the other with binding energy of 531.0–531.4 eV (O_{sur}), to surface-adsorbed oxygen, such as O_2^{2-} or O^-, sometimes with shoulder peaks at 533.0 eV (O_H) ascribed to hydroxyl species and adsorbed water species presser as contaminants [37]. For CeO_2, binding energy of O_{latt} is 528.9 eV. With the presence of Ti, binding energy of O_{latt} increases due to "Ti ⟵ O" electron-transfer processes [27], through the formation of Ce—O—Ti. That is to say, the mixed oxides are not mixtures of two different oxides but rather a uniform solid solution in which Ti and Ce have chemical interactions [27]. As a result, the behavior of O_{latt} species can be affected by Ce—O—Ti. Moreover, the ratio of O_{sur}/O_{total} (estimated by peak area) decreases with the decrease in Ce species (Table 2), indicating that the contribution to O_{sur} is mainly from CeO_2. As known, CeO_2 possesses a considerable amount of active surface oxygen chemically adsorbed on the vacancies (O^-). The shift of O_{sur} binding energy further suggests chemical interaction of Ti species with Ce species.

NH_3-TPD profiles of $Ce_{1-x}Ti_xO_2$ samples shown in (Fig. 6A) can be deconvoluted by the Gauss curve fitting method [38] into three peaks (noted as a, b and c, respectively) with the centers at 217–255, 272–327 and 351–403 °C, corresponding to ammonia desorbed from weak, moderate and strong acidic sites. The area of a specific peak corresponds to the amount of ammonia that desorbs from the sample, and could be taken as a standard to quantify the acidity of the sample [39]. For $Ce_{0.5}Ti_{0.5}$, the areas of "a" peak and "b" peak increase to 53 and 527% of those over CeO_2, respectively (Table 1). Ti species promotes the formation of strong acidic sites (c peak) which approach the maximum over $Ce_{0.5}Ti_{0.5}$. The numerical values corresponding to various acidic strength normalized by surface area increases significantly and keeps almost constant after $R = 0.327$ ($Ce_{0.5}Ti_{0.5}$) (Fig. 6B). As mentioned previously, crystal structure of $Ce_{1-x}Ti_xO_2$ samples becomes distortion, probably with electronic unbalance due to the change in length of Ce—O and Ti—O bonds, which contributes acidity. Additionally, TiO_2 is acidic solid, and it can be expected that $Ce_{1-x}Ti_xO_2$ solid solution possesses much more acidic sites than CeO_2. Thus, the total acidity is proportional to R (Fig. 6B insert). On Py-FTIR spectra of all samples, there appear characteristic peaks of pyridine adsorbed on Lewis acid sites at ca.1441, 1574 and 1601 cm^{-1} (Fig. S5) [40]. Obviously, Ce^{3+}/Ce^{4+} and Ti^{3+}/Ti^{4+} species contribute to Lewis acid sites.

3.2. Activity of $Ce_{1-x}Ti_xO_2$ catalysts

The activity of $Ce_{1-x}Ti_xO_2$ catalysts for *o*-DCB combustion is shown in Fig. 7 as a function of temperature. CeO_2 exhibits a considerable activity with T_{90} (the temperature needed for 90% conversion) of 510 °C (Table 3). With the incorporation of Ti, the activity is remarkably improved and the conversion curves shift to lower temperature, indicating that the formation of $Ce_{1-x}Ti_xO_2$

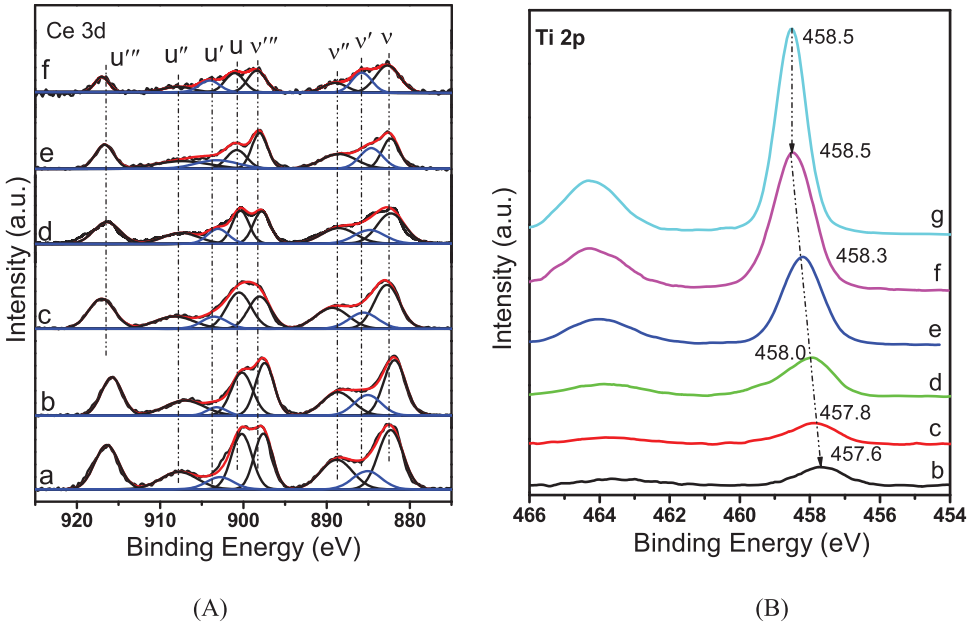

Fig. 5. XPS spectra of Ce 3d (A), O 1s (B), Ti 2p (C) for $Ce_{1-x}Ti_xO_2$ samples; a-CeO_2, b-$Ce_{0.9}Ti_{0.1}$, c-$Ce_{0.7}Ti_{0.3}$, d-$Ce_{0.5}Ti_{0.5}$, e-$Ce_{0.3}Ti_{0.7}$, f- $Ce_{0.1}Ti_{0.9}$ and g-TiO_2.

Table 2
XPS analyses of $Ce_{1-x}Ti_xO_2$ samples.

Sample	Ti/Ti + Ce (atom)	Ce + Ti/O (atom)	Ce^{3+}/Ce (atom)	O_{sur}/O_{total} (atom)	Binding energy of O_{latt} (eV)
CeO_2	0	0.49	12.0	0.50	528.9
$Ce_{0.9}Ti_{0.1}$	0.05	0.52	12.3	0.46	529.1
$Ce_{0.7}Ti_{0.3}$	0.12	0.50	14.2	0.44	529.2
$Ce_{0.5}Ti_{0.5}$	0.33	0.45	17.4	0.42	529.4
$Ce_{0.3}Ti_{0.7}$	0.60	0.40	20.0	0.35	529.6
$Ce_{0.1}Ti_{0.9}$	0.86	0.38	24.0	0.30	529.8
TiO_2	1	0.38	0	0.19	529.8

solid solution is favorable for *o*-DCB combustion. $Ce_{0.5}Ti_{0.5}$ has the highest apparent activity with T_{90} of about 375 °C (Table 3), which is closed to T_{90} obtained over V_2O_5/TiO_2-based catalysts [2,4,19]. Fig. 8 shows that T_{90} decreases quickly with the increase in Ti content for the catalysts with fluorite structure. However, when Ti content is high enough to form monocline and anatase structure, T_{90} rises from 376 to 442 °C, indicating that the island TiO_2 is not favorable for the reaction. Another experiment (Fig. 8) shows that the effect of Ti on the activity for benzene combustion is negative and T_{90} increases with Ti content. T_{90} for benzene over the catalysts with fluorite structure decreases to a large extent, and CeO_2 presents the lowest T_{90}, 267 °C. This phenomenon indicates

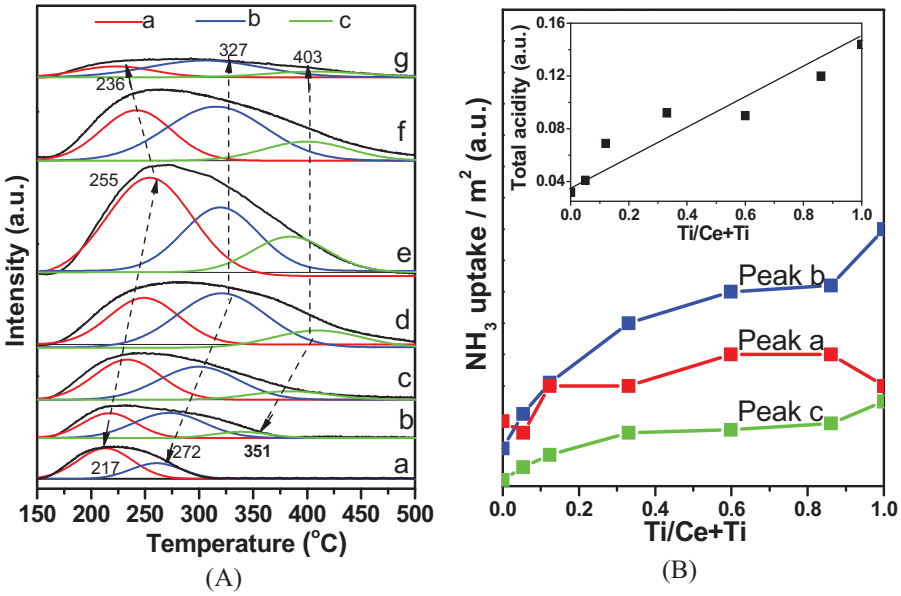

Fig. 6. NH_3-TPD profiles of $Ce_{1-x}Ti_xO_2$ samples and total acidity versus the ratio of Ti/Ce + Ti(insert); a-CeO_2, b- $Ce_{0.9}Ti_{0.1}$, c-$Ce_{0.7}Ti_{0.3}$, d- $Ce_{0.5}Ti_{0.5}$, e-$Ce_{0.3}Ti_{0.7}$, f- $Ce_{0.1}Ti_{0.9}$ and g-TiO_2.

Table 3
The activity of $Ce_{1-x}Ti_xO_2$ catalysts with various ratios of Ti/Ce + Ti.

Sample	*o*-DCB					B		CB	
	T_{90} (°C)	Rate[a] (μmol/m² min)	TOF_{Ti}[b] (μmol/m² min)	Ea (KJ/mol)	TCB[c] ppm	T_{90} (°C)	Ea (KJ/mol)	T_{90} (°C)	Ea (KJ/mol)
CeO_2	500 (547)[d]	0	0	122.5 (160.0)[d]	58 (30)[d]	267	62.5	483	110.7
$Ce_{0.9}Ti_{0.1}$	433 (449)	0.034	0.640	118.2 (84. 2)	29 (12)	274	73.4	410	106.3
$Ce_{0.7}Ti_{0.3}$	394 (426)	0.056	0.455	83.6 (80.6)	6 (ND)	322	84.7	383	78.5
$Ce_{0.5}Ti_{0.5}$	375 (373)	0.053	0.160	95.7 (74.1)	2 (ND)	377	94.1	357	70.1
$Ce_{0.3}Ti_{0.7}$	396 (420)	0.029	0.048	102.1 (89.0)	ND (ND)	405	105.3	375	118.3
$Ce_{0.1}Ti_{0.9}$	433 (–)	0.024	0.028	116.0 (–)	ND (–)	440	120.4	410	125.9
TiO_2	>600 (–)	0	0	–	5	–	–	–	–

[a] The rate calculated based on the mole of *o*-DCB transformed per minute and per square meter from *o*-DCB conversion at 275 °C under the reaction condition described in Fig. 9.
[b] TOF_{Ti} calculated based on the mole of *o*-DCB transformed per minute and per square meter normalized by Ti% obtained form XPS data.
[c] Maximum of trichlorobenzene within the experimental temperature range.
[d] The results obtained in wet feed.

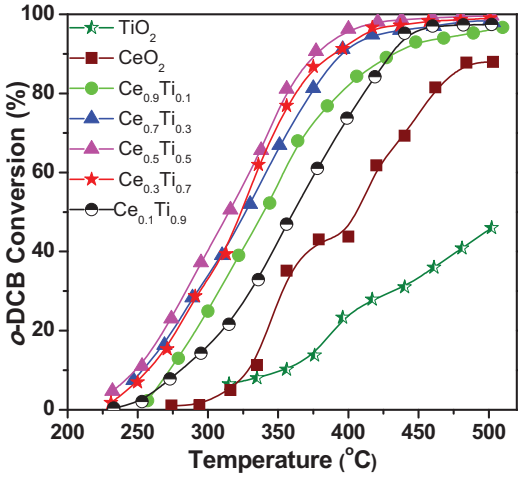

Fig. 7. *o*-DCB conversion over $Ce_{1-x}Ti_xO_2$ catalysts; *o*- DCB concentration, 1000 ppm; GHSV = 30,000 h^{-1}; catalyst amount, 200 mg.

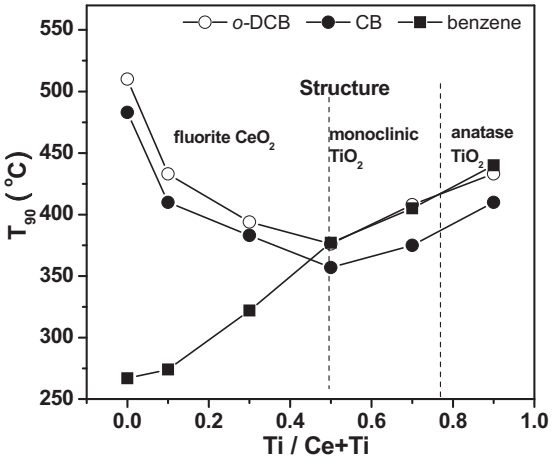

Fig. 8. T_{90} for benzene, CB and *o*-DCB combustion over $Ce_{1-x}Ti_xO_2$ catalysts; reactant concentration, 1000 ppm; GHSV = 30,000 h^{-1}; catalyst amount, 200 mg.

that Cl species could retard the reaction over CeO_2-based catalysts [18]. Recently, Teschner et al. found that during the gas-phase HCl oxidation ($4HCl + O_2 \rightarrow 2Cl_2 + 2H_2O$) over ceria, under low oxygen over- stoichiometry, ceria was prone to a certain extent to subsurface/bulk chlorination, which leaded to deactivation, probably due

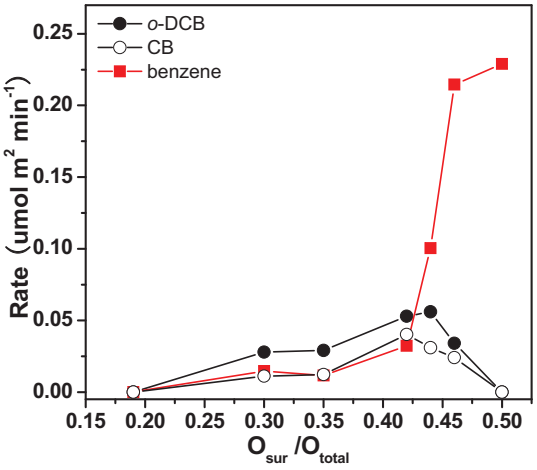

Fig. 9. The reaction rate versus O_{sur}/O_{total} at 275 °C over catalysts for *o*-DCB, CB and benzene combustion based on the mole number of converted reactant per square meter per minute; reactant concentration, 1000 ppm; GHSV = 30,000 h^{-1}; catalyst amount, 200 mg.

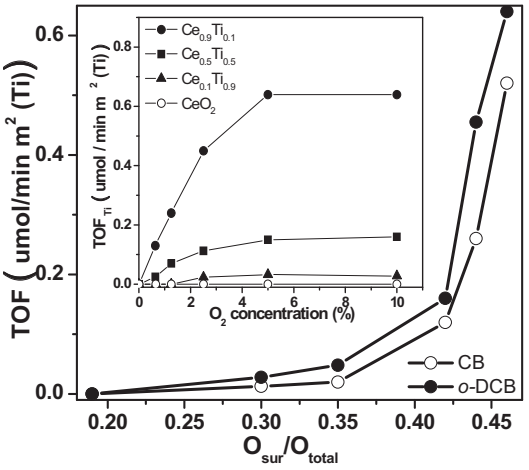

Fig. 10. TOF_{Ti} at 275 °C versus O_{sur}/O_{total} (at 10% O_2) and oxygen concentration (insert, for *o*-DCB oxidation) over the catalysts; reactant concentration, 1000 ppm; GHSV = 30,000 h^{-1}; catalyst amount, 200 mg.

to inhibition for ceria from oxygen activation with a high surface chlorination degree (strongly suggested by Electron Paramagnetic Resonance experiments) [41]. As previously reported, the addition of Ru [42] or Mn [7] species into CeO_2 reduced Cl deposition through increase in surface oxygen and thus promoted really CB combustion. The effect of Ti—O—Ce could be related to the removal of Cl species from the surface of catalysts, which is confirmed by CO_2-TPD and XPS in later section. Considering the effect of surface area on the reaction, the rate at 275 °C was calculated based on the mole of *o*-DCB transformed per minute and per square meter. The rate increases with Ti content and reaches the highest with the substitution of Ti for Ce in fluorite structure approaching to saturation (R = 0.3–0.5) (Table 3). The contribution to rate would be mainly from the reaction occurring on the active sites related to Ti species or Ti—O—Ce, because CeO_2 presents no activity below 275 °C (Fig. 7).

As known, the surface active oxygen is crucial for the oxidation of CVOCs [43]. To learn the action of active oxygen in benzene/CB/DCB oxidation, the correlation of rate with O_{sur}/O_{total} was investigated. For the catalysts with R = 0.5 or higher, the rate increases with O_{sur}/O_{total} (Fig. 9). The presence of Ce species seems to improve the activity for aromatics oxidation of Ti-rich catalysts through the increase in active oxygen. For catalysts with fluorite structure, the rates for CB and *o*-DCB decrease, while the rate for benzene oxidation shows a rapid increasing trend, indicating that the controlling step for chlorinated aromatics is not related to O_{sur}/O_{total}. Considering that CeO_2 presents no activity below 275 °C and the modification of CeO_2 with transitional metals is often localized [44] , TOF_{Ti} based on the rate per square meter normalized by Ti% on surface obtained from XPS data can be used for comparing activity difference among Ti—O—Ce or Ti species. Fig. 10 shows TOF_{Ti} at 275 °C as a function of O_{sur}/O_{total} and oxygen content (insert). Within an oxygen content range of 0–10%, TOF_{Ti} increases with oxygen content and rapidly with Ce content at a given oxygen content except for CeO_2. At 10% O_2 at 275 °C, TOF_{Ti} of the catalysts with fluorite structure increases rapidly with O_{sur}/O_{total}, because there are clusters of Ce species around Ti—O—Ce, on which oxygen can be dissociated and activated more effectively. $Ce_{0.9}Ti_{0.1}$ presents the highest TOF_{Ti} of 0.64 μmol min^{-1} m^{-2} (Ti). For Ti-rich catalysts, TOF_{Ti} present low value, due to a small amount of sites which activate oxygen [22], for example, 0.028 μmol min^{-1} m^{-2} (Ti) on $Ce_{0.1}Ti_{0.9}$. Therefore, the dependence of activity on oxygen content decreases with the increase in Ti.

Additionally, the rate for the combustion of CB and *o*- DCB increases with the total acid amount of catalysts with fluorite structure (Fig. S6), which is related to the adsorption of chlorinated aromatic molecules on acidic sites (confirmed with later situ-FT-IR analyses). Moreover, new acidic sites should be the contribution from Ti^{3+}/Ti^{4+} species which are significantly resistant to Cl adsorption. For Ti-rich catalysts, the activity is not dependent on the total acid amount (Fig. S6), because their ability for activating oxygen is poor and an oxidation step is rather slow.

Assuming the concentration of reactants having no significant change within 20% conversion, the temperature dependence of rate can be used to find apparent activation energies (Ea) (Fig. S7), and the associated Ea values with 95% confidence limits are listed in Table 3. Ea estimated from the rate for *o*-DCB oxidation is 122.5 KJ/mol for CeO_2. CeO_2 has been identified as an efficient catalyst for HCl oxidation (Deacon reaction) in the temperature range of 350–450 °C with Ea of 70–90 KJ/mol [45,46]. From the result that CeO_2 is highly active for the oxidation of aromatics (Ea = 62.5 KJ/mol for benzene (Table 3)), it seems reasonable to consider that Cl removal as Cl_2 is the rate-controlling-step for *o*-DCB oxidation over CeO_2. The incorporation of Ti can promote Cl removal and $Ce_{0.7}Ti_{0.3}$ catalyst presents the lowest Ea of 83.6 KJ/mol. Further increasing Ti content, Ea presents an increasing trend, indicating that the oxidation step becomes slow due to the decrease in surface active oxygen. Additionally, Ea for benzene oxidation (Table 3) increases with Ti content, indicating that the activity of Ti—O—Ce species for oxidation of aromatics is not high. It can be concluded that high activity of $Ce_{1-x}Ti_xO_2$ catalysts can be ascribed to an effective combination of Cl removal and oxidation.

3.3. Distribution of products

TPSR analyses (Fig. S8) for products in the effluent show that main products are CO, CO_2, HCl and Cl_2. The formation of Cl_2 was not observed until 300 °C. The selectivity for Cl_2 increases with temperature from 250 to 400 °C (Fig. S9). Cl balance reaches 85% or more. For Deacon reaction ($HCl + O_2 \rightarrow Cl_2 + H_2O$), TiO_2 is inactive, on which almost no Cl_2 was detected. However, the addition of TiO_2 into CeO_2 can promote the formation of Cl_2 to some extent, probably through the modification of Cl_2 adsorption strength [42], and the selectivity for Cl_2 is in a range of 20–35% at 390 °C (Fig. S9). For the products of *o*-DCB chlorination, only 1,2,4,-TCB is detected at 250 °C or higher (Fig. 11), indicating that the chlorination of *o*-DCB occurs via a classical aromatic electrophilic substitution

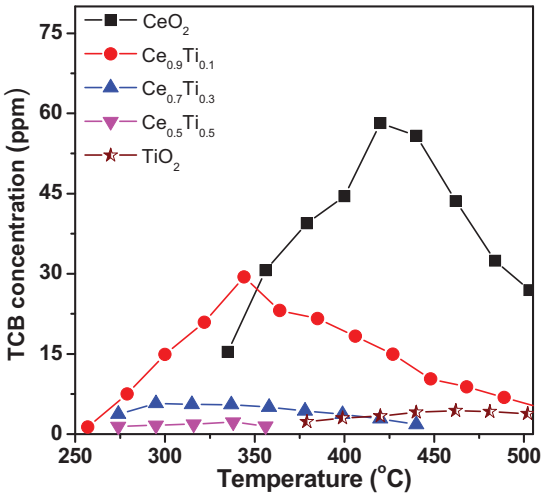

Fig. 11. TCB distributions for *o*-DCB combustion over catalysts; *o*-DCB concentration, 1000 ppm; GHSV = 30,000 h^{-1}; catalyst amount, 200 mg.

mechanism [46]. $Ce_{0.9}Ti_{0.1}$, $Ce_{0.7}Ti_{0.3}$ and $Ce_{0.5}Ti_{0.5}$ present a similar temperature range for TCB distribution (250–500 °C) (Fig. 11), with TCB maxima of 30.0, 5.0 and 1.5 ppm, respectively. While TCB maximum up to 59 ppm is detected on CeO_2, although an initial temperature for TCB formation shifts to 325 °C. This is related to the formation of reactive inorganic Cl species at higher temperature. No TCB was detected on $Ce_{0.3}Ti_{0.7}$ and $Ce_{0.1}Ti_{0.9}$ within a detection limitation of FID. Obviously, clusters of CeO_2 species could be responsible for the chlorination. In the case of CB combustion, similar results are observed and much higher *o*-DCB/*p*-DCB maximum is formed on CeO_2 (Fig. S10). XPS analyses for the used catalysts show that the binding energy of Cl 2p of inorganic Cl species decreases with Ti content and for $Ce_{0.3}Ti_{0.7}$ and $Ce_{0.1}Ti_{0.9}$, is 198.2 ± 0.1 eV, lower than that of CeO_2 (198.7 eV) (Fig. S11), indicating that the strength of Cl adsorption can be modified by Ti. Low activity for chlorination of *o*-DCB over $Ce_{1-x}Ti_xO_2$ could be related likely to the decrease in binding energy of Cl 2p.

3.4. Catalyst stability and characterization of the used catalysts

Fig. 12A presents the experimental results of the stability test at 330 °C. This test was carried out after the evaluation of activity of the fresh catalysts. Stable activity can be achieved within 50 h. CeO_2, $Ce_{0.9}Ti_{0.1}$, $Ce_{0.7}Ti_{0.3}$, $Ce_{0.5}Ti_{0.5}$, $Ce_{0.3}Ti_{0.7}$, $Ce_{0.1}Ti_{0.9}$ and TiO_2 present a stable conversion of 17, 41, 50, 66, 56, 47 and 5%, respectively. It is necessary for reactions involving an aggressive reaction mixture such as HCl to increase the duration of stability test [47–49]. $Ce_{0.7}Ti_{0.3}$, $Ce_{0.5}Ti_{0.5}$ and $Ce_{0.3}Ti_{0.7}$ in particular were tested for another 100 h at 375 °C with the conversion as high as 90, 80 and 85%, respectively (Fig. 12B). During stability test, the product selectivity keeps almost constant, indicating that the structures of active sites are stable. It is generally thought that the accumulation of Cl species on Ce-based catalysts can result in a loss in activity [42] . XPS (Fig. S11) and EDS analyses confirm that Cl deposition on the used catalysts increases with Ce content (Table 4). CO_2-TPD test shows (Fig. S12) that there are strong peaks of CO_2 desorption from the surface of fresh CeO_2 at 180 °C, but CO_2 does not show a significant interaction with the chlorinated surface of the used CeO_2, on which almost no CO_2 desorption is observed. While the peak intensity of the used $Ce_{0.9}Ti_{0.1}$ decreases to some extent. As known, a significant part of basic sites on metal oxides generally resulted from surface basic lattice O sites, which can be exchanged by chloride during Deacon reaction ($2HCl + O_2 \rightarrow Cl_2 + H_2O$) [50]. Adding Ti into CeO_2 will increase oxygen bonding energy (Fig. 5C)

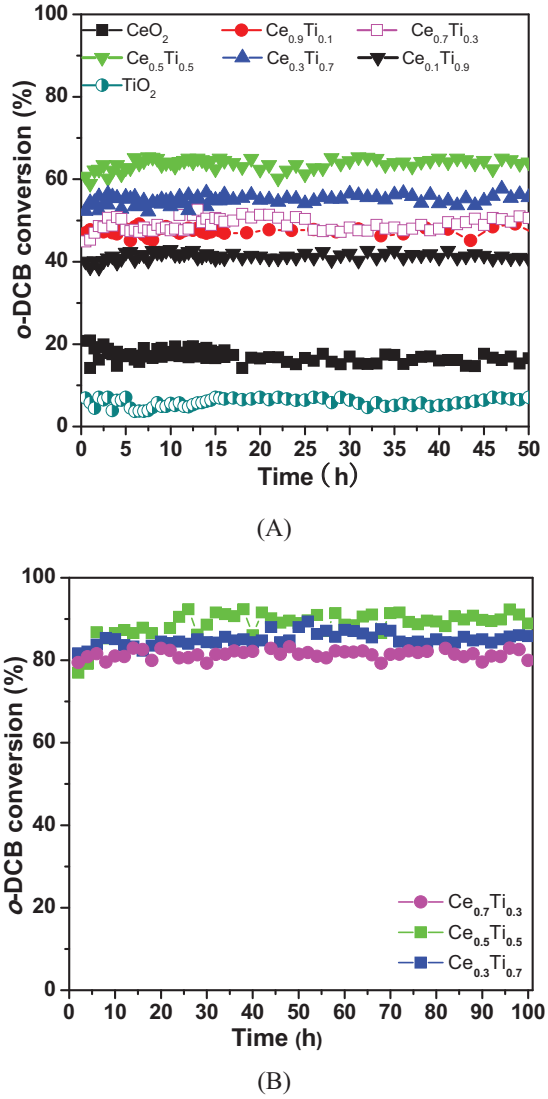

Fig. 12. The activity for *o*-DCB catalytic combustion over $Ce_{1-x}Ti_xO_2$ catalysts on stream feed at 330 °C (A) and 375 °C (B); *o*-DCB concentration, 1000 ppm; GHSV = 30,000 h^{-1}; catalyst amount, 200 mg.

and decrease the electron density around oxide ion. As a result, the basicity of these lattice O sites can be decreased, and the exchange of chloride becomes difficult. The rate on CeO_2 is enhanced at 350 °C or higher, where Cl species is removed through Deacon reaction. On the other hand, H_2 consumption in H_2-TPR test (Fig. S13) on the used CeO_2 decreases by 64% (Table 4), while for the used catalysts containing Ti, decreases to a much smaller extent. XPS characterization shows that the ratios of O_{sur}/O_{total} decrease to a different extent (Table 4). The catalysts with fluorite structure present 10-11% decrease in O_{sur}/O_{total}. The corresponding result is the increase in Ce^{3+}/Ce ratio, which results from the formation of CeOCl [51]. For Ti-rich catalysts, O_{sur}/O_{total} decreases to a smaller extent, due to the chlorination of Ti species [22]. Additionally, a peak with binding energy of 199.5–200.5 eV on XPS spectra of Cl 2p was observed (Fig. S11C), which can be ascribed to Cl atom of *o*-DCB [52]. The amount of organic Cl species increases significantly with Ti content (Table 4), implying that more *o*-DCB molecules adsorbed on Ti^{4+} sites (confirmed by later in situ FT-IR results). Slight changes in the element compositions on surface are owing to the modification of chemical environment by the presence of chlorine. No changes in structure and physical parameters of the used $Ce_{1-x}Ti_xO_2$ catalysts can be found. Therefore, it can be deduced that low activity of CeO_2

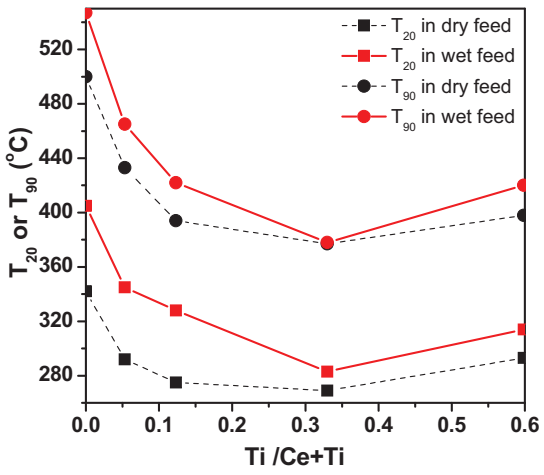

Fig. 13. T_{90} for *o*-DCB combustion over $Ce_{1-x}Ti_xO_2$ catalysts; *o*-DCB concentration, 1000 ppm; 10% O_2, 1.5% (*V*/*V*) H_2O and N_2 balance; GHSV = 30,000 h^{-1}; catalyst amount,200 mg.

or $Ce_{1-x}Ti_xO_2$ catalysts with very low Ti content for the oxidation of CB and *o*-DCB can be due to the exchange of chlorine for basic lattice oxygen.

3.5. The effect of water

It is necessary to investigate the effect of water on the activity of catalysts for *o*-DCB combustion. The conversion of *o*-DCB over $Ce_{1-x}Ti_xO_2$ catalysts was investigated in the presence of 1.5% (*V*/*V*) water (Fig. S14). The negative effects of water on *o*-DCB conversion were observed, especially at low temperature (Fig. 13). For the catalysts with fluorite structure, T_{20} and T_{90} significantly rise with the increase in Ce content, while Ti-rich catalysts present slight increase. It seems that Ti species can resist water more effectively. Herman et al. found that H_2O can not adsorb on anatase TiO_2 <1 0 1> at 300 K or higher [53]. Lykhach et al. found the existing of hydroxyl groups on CeO_2 at 700 K in SRPES spectra [54]. $Ce_{0.9}Ti_{0.1}$, $Ce_{0.7}Ti_{0.3}$ and $Ce_{0.5}Ti_{0.5}$ present TOF_{Ti} at 300 °C of 0.17 ± 0.02 μmol min^{-1} m^{-2} (Ti), while in dry feed under the similar condition, 1.32, 0.77 and 0.27 μmol min^{-1} m^{-2} (Ti), respectively. For $Ce_{0.3}Ti_{0.7}$, a slight change in TOF_{Ti} can be observed, although TOF_{Ti} is down to 0.04 μmol min^{-1} m^{-2} (Ti). For the catalysts containing Ti, Ea calculated based on the rate in wet feed is in a range of 74.1–89.0 KJ/mol (Table 3). These results suggest that the active sites for reaction in wet feed be related to Ti species. TiO_2 has not a significant activity until 300 °C (Fig. S14). Here, oxygen must be activated on interface Ti—O—Ce species. The effect of H_2O may be caused by competition of OH^- groups produced during H_2O dissociation with *o*-DCB for active sites. Raising temperature, H_2O adsorption becomes weak, and thus the corresponding retardancy decreases. A large difference between TOF_{Ti} in dry and wet feeds for the catalysts with low Ti content indicates that Ce species around Ti—O—Ce should affect the resistance of Ti species to the attack by water. On the other hand, water can remove chloride through providing H^+ and retard Deacon reaction ($HCl + O_2 \rightarrow Cl_2 + H_2O$). As a result, TCB maximum on CeO_2 and $Ce_{0.9}Ti_{0.1}$ decreases down to 30 and 12 ppm. The effect of water on the oxidation of chlorinated aromatics has also been studied on some other occasions [55,56] . Amiridis found that water promoted the reaction at low temperature through the removal of Cl species and C species on the surface, but it inhibited at high temperature the oxidation of dichlorobenzene over V_2O_5/TiO_2 catalysts due to the adsorption of water on the active sites [57]. Bertinchamps et al. observed that the addition of water decreased the number of strong Brönsted acid sites involved in the adsorption of chlorobenzene [58].

3.6. *In situ FTIR spectra of* o-*DCB adsorption and oxidation*

3.6.1. DCB adsorption

FTIR spectra collected at different temperatures over CeO_2 are shown in Fig. 14A. The bands at 1573, 1455, 1445 and 1434 cm^{-1} can be assigned to the C=C degenerated stretching vibrations of the aromatic ring [59]. The band at 1573 cm^{-1} is shifted slightly from the 1588 cm^{-1} positions for gas-phase *o*-DCB. In a similar example of CB adsorption on TiO_2 [60], the gas-phase band at 1588 cm^{-1} was shifted to 1582 cm^{-1}, an effect attributed to the formation of a π-complex between surface Ti^{4+} ions and the aromatic ring. A similar mechanism can be proposed for *o*-DCB adsorption on Ce^{4+}/Ce^{3+} ions. Spectra of the hydroxyl region (Fig. S14A) suggest that the adsorption of *o*-DCB affects the surface hydroxyl groups of CeO_2 at 150–400 °C, whereas spectra exhibit negative bands in a range of 3722–3582 cm^{-1}, which usually were assigned to strong surface hydroxyl groups. Weak bands at 1240 and 1225 cm^{-1} corresponding to phenolates are observed at 200 °C. Previous investigations proposed that the first step in the catalytic oxidation of chlorinated benzenes over V_2O_5/TiO_2 catalysts was a nucleophilic substitution [20], during which the chlorine atom was abstracted and replaced by O^{2-} ions and residual surface hydroxyl groups associated with each metal, forming different intermediates (i.e., phenolates and catecholates). It can be expected that the consumption of Ce—OH groups during *o*-DCB adsorption is related to the formation of phenolates or catecholates. These bands become weak at 300 °C, while new bands appear at 1368 and 1560 cm^{-1} (assigned to carbonate

Table 4
The surface compositions[a] and H_2 uptake of the used catalysts[b].

Sample	Ti/Ti + Ce (atom)	Ti + Ce/O (atom)	Cl			Ce^{3+}/Ce	O_{sur}/O_{total}	H_2 uptake (m mol/g)
			Total[c](%)	Inor.[d](%)	Or.[d](%)			
CeO_2	0	0.55	3.5	3.1	0.5	17.5	0.45 (−10.1%)[e]	0.12
$Ce_{0.9}Ti_{0.1}$	0.05	0.53	3.4	2.6	0.9	17.8	0.42 (−11.0%)	0.20
$Ce_{0.7}Ti_{0.3}$	0.13	0.49	2.1	2.3	0.8	18.1	0.41 (−11.0%)	0.31
$Ce_{0.5}Ti_{0.5}$	0.39	0.41	1.8	1.4	0.8	19.2	0.39 (-11.0%)	0.31
$Ce_{0.3}Ti_{0.7}$	0.63	0.37	1.5	1.4	0.9	23.5	0.33 (−5.7%)	0.28
$Ce_{0.1}Ti_{0.9}$	0.87	0.33	1.1	1.0	1.2	34.2	0.28 (-6.7%)	0.14
TiO_2	0	0.33	0	0.4	0.2	0	0.20 (−9.1%)	–

[a] The values determined by XPS.
[b] The used catalysts for 1000 min under reaction condition as described in Fig. 13A.
[c] Cl deposition determined by EDS.
[d] Cl deposition determined by XPS.
[e] The changes compared with the values of the fresh catalysts.

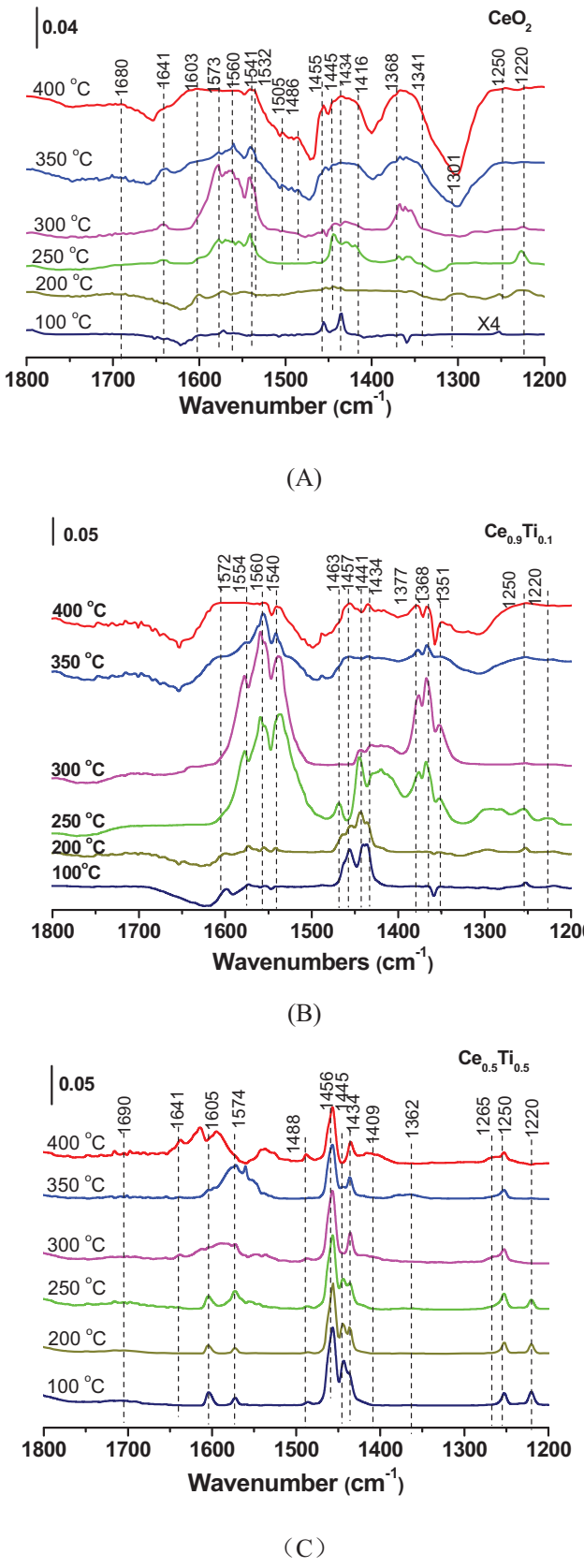

Fig. 14. In situ FTIR spectra of CeO_2, $Ce_{0.9}Ti_{0.1}$ and $Ce_{0.5}Ti_{0.5}$ catalysts collected at different temperature on a stream of 1000 ppm *o*-DCB, N_2 for 0.5 h.

bidentate), 1434 and 1541 cm^{-1} (asymmetric stretching vibration of carboxylates with the acetate type [19,61–63]) and 1341 and 1532 cm^{-1} (formates, acetates, and maleates), indicating that phenolates are intermediates for *o*-DCB oxidation over CeO_2. This result is similar to that of *o*-DCB oxidation over Mn-modified Co_3O_4 catalysts [16]. Additionally, It is interesting to find that the intensity of new bands appearing at 1680–1700 and 1368 cm^{-1} increase with temperature, suggesting the presence of adsorbed species different from that related to bands at 1578, 1475, and 1444 cm^{-1}. In addition to π bonding, the undissociated *o*-DCB molecules are likely further stabilized via hydrogen bonding (confirmed by the appearance of a negative band at 3705–3657 cm^{-1}), whereas the presence of surface oxygen in the form of O^{2-} ions, surface basic lattice oxygen O^{2-} clusters may be responsible for acid-base-type interactions yielding another species [64,65]. Raising temperature up to 350 °C or higher, these bands become strong, due to the increase in basic lattice oxygen O^{2-} through removal of Cl as Cl_2 (Deacon reaction becomes significant until 300 °C).

At 200–400 °C, a weak peak at 1638 cm^{-1} is observed, accompanied by the appearance of strong peak at 1419 and weak peak at 1301 cm^{-1}. These peaks can be attributed to a surface enolic species. Additional bands at 2939 and 2867 cm^{-1} ascribed to C═C and —CH— are also the present in the spectra of adsorbed *o*-DCB, which further verifies the formation of the enolic form [66]. The bands corresponding to the enolic form were not observed in CB adsorption on CeO_2 [23], indicating that the ability of oxidation for CeO_2 decreases in *o*-DCB reaction. Moreover, partially oxidized products such as formates, acetates, and maleates were observed, further confirming that the increase of Cl substitution makes reaction more difficult. Oxidation products were seen in the absence of gas-phase oxygen, indicating involvement in surface oxygen including hydroxyl groups in the oxidation process [20,60]. It should be pointed that the weakness in intensity of bands ascribed to *o*-DCB adsorption may be related to the exchange of chloride with basic surface lattice oxygen on CeO_2, on which Cl species can not be removed until 300 °C (Fig. S8). On the other hand, negative bands in hydroxyl region observed probably result from the substitution of Cl species for hydroxyl during the decomposition of *o*-DCB, which also make the adsorption of *o*-DCB become difficult.

In *o*-DCB oxygen-free feed, the spectra obtained on $Ce_{0.9}Ti_{0.1}$ and $Ce_{0.5}Ti_{0.5}$ include bands similar to those for *o*-DCB adsorption and oxidation (Fig. 14B and 14C). However, the bands at 1573, 1455 and 1434 cm^{-1} for *o*-DCB adsorption clearly split into two groups of bands at 1573, 1455, 1434 cm^{-1} and 1572, 1462, 1432 cm^{-1}, respectively. These splits could suggest *o*-DCB adsorption on two different types of sites associated with Ce and Ti species. With the increase in Ti amount, the intensity of *o*-DCB adsorption in the form of π-complex becomes strong, indicating that Ti species is favorable for *o*-DCB adsorption, due to the production of new strong acidic sites (Fig. 6). Spectra of the hydroxyl region exhibit the shift of negative bands from 3722 to 3582 cm^{-1} for CeO_2 to 3742–3644 cm^{-1} (centred at 3686 cm^{-1}) for $Ce_{0.5}Ti_{0.5}$, along with a positive band at 3586 cm^{-1} which become strong with Ti content (Fig. S15). These spectra suggest that the presence of Ti promotes the adsorption of *o*-DCB molecules through a dual-site interaction (i.e., OH···π-electron and OH···Cl), leading to the formation of weaker hydrogen-bonded OHs [67,68], and there are more hydroxyl groups available to the adsorption of *o*-DCB molecules. The band at 3686 cm^{-1} is attributed to hydroxyl groups near Ti species which can not be substituted by chloride and can be recycled by the water produced during reaction. Thus, the adsorption of *o*-DCB on the catalysts containing Ti can be promoted by Ti—OH, although the amount of their basic surface lattice oxygen decreases.

Additionally, the bands at 1368 and 1560/1556 cm^{-1} (carbonate bidentate), 1434 and 1540 cm^{-1} (asymmetric stretching vibration of carboxylates with the acetate type), and 1341 and 1535 cm^{-1} (formates, acetates, and maleates) were also observed and become significantly weak at any given temperature with the increase in Ti content (Fig. 14B and 14C). Furthermore, surface enolic species characteristic bands at 1638, 1419 and 1301 cm^{-1} are not observed. In the absence of gas oxygen, the formation of partially oxidized products is involvement in surface oxygen. As mentioned in characterization section, active surface oxygen is in an inverse proportion to Ti/Ce + Ti ratio and the mobility of oxygen in Ce—O—Ti solid solution becomes significant only at 400 °C or higher (Fig. 4), and thus the presence of Ti almost can not promote oxidation step at low temperature.

3.6.2. DCB oxidation

For the feed containing all reactants, the bands at 1573, 1455, 1464 and 1435 cm^{-1} on IR spectra observed at 100 °C over CeO_2, $Ce_{0.9}Ti_{0.1}$ and $Ce_{0.5}Ti_{0.5}$ are ascribed to *o*- DCB adsorption as mentioned above (Fig. 15). For CeO_2, the bands of *o*-DCB adsorption and containing-oxygen intermediates such as phenolate and enolic species become strong. And the bands ascribed to carboxylates grow in intensity (Fig. 15A). These results indicate that the presence of gas oxygen promotes *o*-DCB adsorption and oxidation on CeO_2. The catalysts containing Ti present similar spectra to those obtained in free oxygen feed, indicating that the formation of adsorbed species containing oxygen involves only in surface oxygen. However, on the spectra of $Ce_{0.5}Ti_{0.5}$ (Fig. 15C), these bands are much weaker than those obtained on CeO_2 and $Ce_{0.9}Ti_{0.1}$ spectra (Fig. 15B), although the bands ascribed to *o*-DCB adsorption is strong. The presence of Ti should be not favorable for the oxidation step, because of the decrease in surface oxygen available. According to the fact that high apparent activity of $Ce_{0.5}Ti_{0.5}$ was observed in the paralleled reaction, it can be expected that *o*-DCB molecules can be activated on strong acidic sites so highly to be oxidized completely through a different reaction way from those on CeO_2. Thus, strong bands of adsorbed species containing oxygen observed on $Ce_{0.9}Ti_{0.1}$ can be ascribed to the species produced on Ce species.

Partial oxidation products were seen in both the presence and absence of gas-phase oxygen, indicating involvement of surface oxygen in the oxidation process. As shown in O_2-TPD experiments (Fig. 4B), different types of oxygen species are present on the surface of $Ce_{1-x}Ti_xO_2$ catalysts. The roles of surface oxygen species on the catalytic oxidation of organic compounds have been explored extensively [69,70]. Electrophilic oxygen species with different stabilities and chemical reactivity are associated with molecularly adsorbed O_2 and partially reduced oxygen species, such as O_2^{2-} and O^-. In contrast, O^{2-} lattice oxide ions are considered as nucleophilic reactants [69]. Furthermore, two hydroxide species, Ce—OH and Ti—OH, are present on the surface of $Ce_{0.9}Ti_{0.1}$ and $Ce_{0.5}Ti_{0.5}$, as indicated by FTIR results (Fig. S16). These species involving oxygen can react with adsorbed *o*-DCB to form varied oxidized products observed in the presence of either surface or gas-phase oxygen. On the sites of CeO_2 with a large amount of active oxygen species (such as O_2^- and O^- adsorbed in vacancies), the oxidation is considerably effective and oxidation products are composed mainly of carbonate bidentate and carboxylic species. However, there are not enough active oxygen species for the sites of $Ce_{0.5}Ti_{0.5}$, on which partial oxidation products exist in a relatively small amount. On the other hand, the presence of Ti maintains surface basic lattice oxygen (nucleophilic sites) for the catalysts containing low Ti content, such as $Ce_{0.9}Ti_{0.1}$ (Fig. S12), and thus promotes *o*-DCB adsorption and activation. More important, the presence of Ti generates additional strong Lewis acidic sites which greatly promote the adsorption and activation of *o*-DCB. Most adsorbed *o*-DCB species can be oxidized

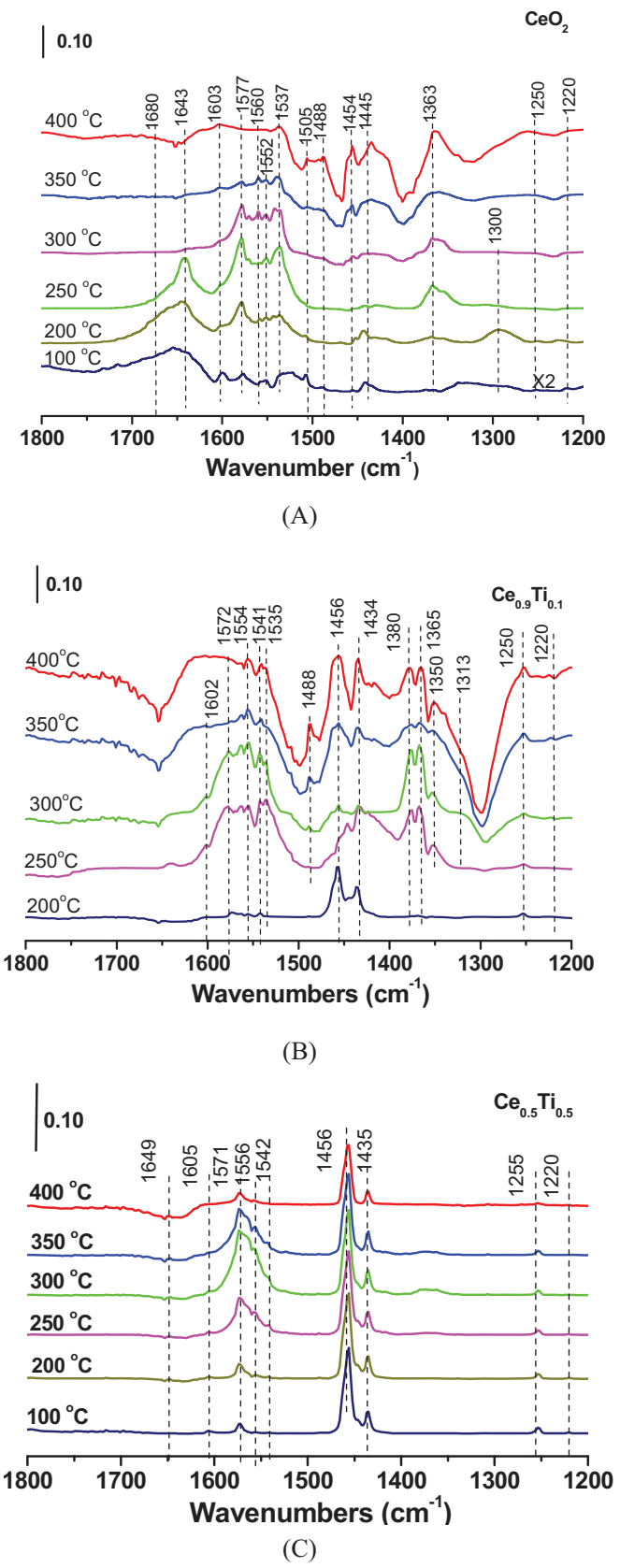

Fig. 15. In situ FTIR spectra of CeO_2, $Ce_{0.9}Ti_{0.1}$ and $Ce_{0.5}Ti_{0.5}$ catalysts collected at different temperature on a stream of 1000 ppm *o*-DCB, 10% O_2 and N_2 for 0.5 h.

effectively to gas-phase reaction products, CO or CO_2. Because of modification in BE of Cl 2p deposited on catalyst surface by Ti incorporation, chlorination of *o*-DCB is greatly retarded. Therefore, $Ce_{1-x}Ti_xO_2$ catalysts with a suitable Ti content, which can provide enough surface oxygen available for the oxidation, present high activity for the oxidation of B, CB and DCB and high selectivity for CO or CO_2. In order to obtain deep insights into this reaction at a molecular level, a mechanism over effective $Ce_{1-x}Ti_xO_2$ catalysts consisting of six elementary steps is schematized: (1) the formation of π-complex of *o*-DCB adsorption during the interaction of *o*-DCB with common Lewis acid sites (Ce^{3+}/Ce^{4+} and Ti^{4+}) and with Ce—OH and Ti—OH, (2) chlorine abstraction by nucleophilic oxygen (basic lattice oxide ions or hydroxyl groups) to form phenolate intermediate, (3) adsorption of the gas- phase oxygen on the surface to replenish the consumed oxygen, (4) the attack of active surface oxygen species (such as O_2^- and O^- adsorbed in vacancies) to aromatic ring, (5) the formation of oxygenate species, such as carbonate bidentate and partially oxidized surface species such as formates, acetates, maleates, carboxylates of the acetate type; (6) further effective reaction of oxygenate species to form gas-phase reaction products (CO_2, CO, H_2O, HCl and Cl_2) (Fig. S8).

4. Conclusion

$Ce_{1-x}Ti_xO_2$ catalysts prepared by sol–gel way were characterized by XRD, HRTEM, Raman, XPS, H_2-TPR, NH_3-TPD and CO_2-TPD, and used in catalytic combustion of *o*-DCB. The experimental results showed that $Ce_{1-x}Ti_xO_2$ catalysts were identified as the forms of fluorite, monocline and anatase. The surface area increases with Ti content, consistent with the increase in distortion extent. All catalysts present Lewis acidity which can be greatly promoted by Ti. While the ratio of O_{sur}/O_{total} decreases with Ti content. $Ce_{1-x}Ti_xO_2$ catalysts present considerable activity for *o*-DCB combustion. Apparent activity increases with Ti and the highest TOF based on rate per square meter normalized by Ti was obtained on $Ce_{0.9}Ti_{0.1}$ with fluorite ceria structure. High stable activity of $Ce_{1-x}Ti_xO_2$ was observed at 330 °C for at least 50 h. The presence of Ti promoted greatly the stable activity of Ce-based catalysts through retarding the exchange of chloride for basic lattice oxygen and surface hydroxyl group. For the products of *o*-DCB chlorination, TCB was detected at 225 °C or higher only over the catalysts with $R = 0.5$ or lower. In situ FTIR showed that *o*-DCB adsorption was much stronger on Ti species than Ce species. The presence of gas oxygen promoted *o*-DCB adsorption on Ce species. Different types of partially oxidized products, including the enolic form of aldehyde-type intermediate, were observed because of different types of oxygen species existing on the surface of $Ce_{1-x}Ti_xO_2$ catalysts.

Acknowledgments

This research was supported by National Natural Science Foundation of China (Nos. 21277047, 21477036 and 21307033).

Appendix A. Supplementary data

Supplementary data associated with this article can be found, in the online version, at http://dx.doi.org/10.1016/j.apcatb.2015.07.053.

References

[1] M. Taralunga, B. Innocent, J. Mijoin, P. Magnoux, Appl. Catal. B: Environ. 75 (2007) 139–146.
[2] S. Krishnamoorthy, J.P. Baker, M.D. Amiridis, Catal. Today 40 (1998) 39–46.
[3] B.H. Aristizábal, C. Maya, C.M.d. Correa, Appl. Catal. A: Gen. 335 (2008) 211–219.
[4] J. Choi, C.B. Shin, T.-J. Park, D.J. Suh, Appl. Catal. A: Gen. 311 (2006) 105–111.
[5] K. Poplawski, J. Lichtenberger, F.J. Keil, K. Schnitzlein, M.D. Amiridis, Catal. Today 62 (2000) 329–336.
[6] B.H. Aristizabal, C. Montes de Correa, A.I. Serykh, C.E. Hetrick, M.D. Amiridis, J. Catal. 258 (2008) 95–102.
[7] X.Y. Wang, Q. Kang, D. Li, Appl. Catal. B: Environ. 86 (2009) 166–175.
[8] X.D. Ma, J.S. Shen, W.Y. Pu, H.W. Sun, Q. Pang, J. Guo, T. Zhou, H.Q. Cao, Appl. Catal. A: Gen. 466 (2013) 68–76.
[9] D.A. Aguilera, A. Perez, R. Molina, S. Moreno, A Appl. Catal. B: Environ. 104 (2011) 144–150.
[10] J.I. Gutiérrez-Ortiz, R. López-Fonseca, U. Aurrekoetxea, J.R. González- Velasco, J. Catal. 218 (2003) 148–154.
[11] R. López-Fonseca, B. de Rivas, J.I. Gutiérrez- Ortiz, A. Aranzabal, J.R. González-Velasco, Appl. Catal. B: Environ. 41 (2003) 31–42.
[12] W. Zhao, J. Cheng, L. Wang, J.L. Chu, J.K. Qu, Y.H. Liu, S.H. Li, H. Zhang, J.C. Wang, Z.P. Hao, T. Qi, Appl. Catal. B: Environ. 127 (2012) 246–254.
[13] S.K. Agarwal, J.J. Spivey, J.B. Butt, Appl. Catal. A: Gen. 81 (1992) 239–255.
[14] X.D. Ma, Q. Sun, X. Feng, X. He, J. Guo, H.W. Sun, H.Q. Cao, Appl. Catal. A: Gen. 450 (2013) 143–151.
[15] J.S. Choi, H.K. Youn, B.H. Kwak, Q. Wang, K.S. Yang, J.S. Chung, Appl. Catal. B: Environ. 91 (2009) 210–216.
[16] T. Cai, H. Huang, W. Deng, Q.G. Dai, W. Liu, X.Y. Wang, Appl. Catal. B: Environ. 166–167 (2015) 393–405.
[17] M. Wu, X.Y. Wang, Q.G. Dai, Y.X. Gu, D. Li, Catal. Today 158 (2010) 336–342.
[18] Y. Dai, X.Y. Wang, Q.G. Dai, D. Li, Appl. Catal. B: Environ. 111–112 (2012) 141–149.
[19] S. Krishnamoorthy, J.A. Rivas, M.D. Amiridis, J. Catal. 193 (2000) 264–272.
[20] J. Lichtenberger, M.D. Amiridis, J. Catal. 223 (2004) 296–308.
[21] F. Bertinchamps, M. Treinen, N. Blangenois, E. Mariage, E.M. Gaigneaux, J. Catal. 230 (2005) 493–498.
[22] M.A.G. Hevia, A.P. Amrute, T. Schmidt, J. Pérez-Ramírez, J. Catal. 276 (2010) 141–151.
[23] H. Huang, Y.F. Gu, J. Zhao, X.Y. Wang, J. Catal. 326 (2015) 54–68.
[24] M.F. Luo, J. Chen, L.S. Chen, J.Q. Lu, Z.C. Feng, C. Li, Chem. Mater. 13 (2001) 197–202.
[25] G. Dutta, U.V. Waghmare, T. Baidya, M.S. Hegde, K.R. Priolkar, P.R. Sarode, Chem. Mater. 18 (2006) 3249–3256.
[26] M. Fernández-Garcıía, A. Martınez- Arias, A. Iglesias-Juez, C. Belver, A.B. Hungnía, J.C. Conesa, J. Soria, J. Catal. 194 (2000) 385–392.
[27] S. Watanabe, X. Ma, C. Song, J. Phys. Chem. C 113 (2009) 14249–14257.
[28] F. Arena, G. Trunfio, J. Negro, B. Fazio, L. Spadaro, Chem. Mater. 19 (2007) 2269–2276.
[29] C. Li, K. Domen, K. Maruya, T. Onishi, J. A. C. S. 111 (1989) 7683–7687.
[30] P. Li, C. He, J. Cheng, C.Y. Ma, B.J. Dou, Z.P. Hao, Appl. Catal. B: Environ. 101 (2011) 570–579.
[31] G.S. Wong, J.M. Vohs, Surf. Sci. 498 (2002) 266–274.
[32] K.-D. Schierbaum, Surf. Sci. 399 (1998) 29–38.
[33] H. He, H.X. Dai, C.T. Au, Catal. Today 90 (2004) 245–254.
[34] Z.Q. Zou, M. Meng, Y.Q. Zha, J. Phys. Chem. C 114 (2009) 468–477.
[35] C. Gionco, M.C. Paganini, S. Agnoli, A.E. Reeder, E. Giamello, J. Mater. Chem. A 1 (2013) 10918–10926.
[36] J. Graciani, J.J. Plata, J.F. Sanz, P. Liu, J.A. Rodriguez, J. Chem. Phys. 132 (2010) 104703.
[37] H.C. Yao, Y.F.Y. Yao, J. Catal. 86 (1984) 254–265.
[38] D. Ma, W.P. Zhang, Y.Y. Shu, X.M. Liu, Y.D. Xu, X.H. Bao, Catal. Lett. 66 (2000) 155–160.
[39] N.R. Meshram, S.G. Hegde, S.B. Kulkarni, Zeolites 6 (1986) 434–438.
[40] S.K. Maurya, P. Patil, S.B. Umbarkar, M.K. Gurjar, M. Dongare, S. Rudiger, E. Kemnitz, J. Mol. Catal. A: Chem. 234 (2005) 51–57.
[41] R. Farra, M. Eichelbaum, R. Schlögl, L. Szentmiklósi, T. Schmidt, A.P. Amrute, C. Mondelli, J. Pérez- Ramírez, D. Teschner, J. Catal. 297 (2013) 119–127.
[42] H. Huang, Q.G. Dai, X.Y. Wang, Appl. Catal. B: Environ. 158–159 (2014) 96–105.
[43] S. Krishnamoorthy, M.D. Amiridis, Catal. Today 51 (1999) 203–214.
[44] A.B. Kehoe, D.O. Scanlon, G.W. Watson, Chem. Mater. 23 (2011) 4464–4468.
[45] A.P. Amrute, C. Mondelli, M. Moser, G. Novell-Leruth, N. López, D. Rosenthal, R. Farra, M.E. Schuster, D. Teschner, T. Schmidt, J. Pérez- Ramírez, J. Catal. 286 (2012) 287–297.
[46] R.W. van den Brink, R. Louw, P. Mulder, Appl. Catal. B: Environ. 16 (1998) 219–226.
[47] A.P. Amrute, G.O. Larrazábal, C. Mondelli, J. Pérez- Ramírez, Angew. Chem. Int. Ed. 52 (2013) 9772–9775.
[48] A.P. Amrute, F. Krumeich, C. Mondelli, J. Pérez-Ramírez, Chem. Sci. 4 (2013) 2209–2217.
[49] E.V. Kondratenko, A.P. Amrute, M.-M. Pohl, N. Steinfeldt, C. Mondelli, J. Pérez-Ramírez, Catal. Sci. Technol. 3 (2013) 2555–2558.
[50] R. Farra, S. Wrabetz, M.E. Schuster, E. Stotz, N.G. Hamilton, A.P. Amrute, J. Perez-Ramirez, N. Lopez, D. Teschner, Phys. Chem. Chem. Phys. 15 (2013) 3454–3465.
[51] B. de Rivas, R. López-Fonseca, M.A. Gutiérrez- Ortiz, J.I. Gutiérrez-Ortiz, Appl. Catal. B: Environ. 104 (2011) 373–381.
[52] D.K.D.T. Clark, D.B. Adams, W.K.R. Musgrave, J. Electron. Spectrosc. Relat. Phenom. 6 (1975) 117–134.

[53] G.S. Herman, Z. Dohnálek, N. Ruzycki, U. Diebold, J. Phys. Chem. B 107 (2003) 2788–2795.
[54] Y. Lykhach, V. Johánek, H.A. Aleksandrov, S.M. Kozlov, M. Happel, T. Skála, P.S. Petkov, N. Tsud, G.N. Vayssilov, K.C. Prince, K.M. Neyman, V. Matolín, J. Libuda, J. Phys. Chem. C 116 (2012) 12103–12113.
[55] X.D. Ma, X. Feng, H.Q. Cao, X.Y. Suo, H.W. Sun, M.H. Zheng, Appl. Catal. B: Environ. 147 (2014) 666–676.
[56] X.D. Ma, X.Y. Suo, H.Q. Cao, J. Guo, L. Lv, H.W. Sun, M.H. Zheng, Phys. Chem. Chem. Phys. 16 (2014) 12731–12740.
[57] C.E. Hetrick, F. Patcas, M.D. Amiridis, Appl. Catal. B: Environ. 101 (2011) 622–628.
[58] F. Bertinchamps, A. Attianese, M.M. Mestdagh, E.M. Gaigneaux, Catal. Today 112 (2006) 165–168.
[59] M. Nagao, Y. Suda, Langmuir 5 (1989) 42–47.
[60] M.A. Larrubia, G. Busca, Appl. Catal. B: Environ. 39 (2002) 343–352.
[61] A.A.I.V.E. Suprunov, React. Kinet. Catal. Lett. 33 (1987) 75.
[62] V. Sanchez Escribano, G. Busca, V. Lorenzelli, J. Phys. Chem. 94 (1990) 8945–8950.
[63] P.S. Chintawar, H.L. Greene, J. Catal. 165 (1997) 12–21.
[64] P. Davit, G. Martra, S. Coluccia, J. Jpn. Pet. Inst. 47 (2004) 359–376.
[65] Q. Dai, G.N. Robinson, A. Freedman, J. Phys. Chem. B 101 (1997) 4940–4946.
[66] D.P. Dreoni, D. Pinelli, F. Trifirò, G. Busca, V. Lorenzelli, J. Mol. Catal. 71 (1992) 111–127.
[67] D. Carmello, E. Finocchio, A. Marsella, B. Cremaschi, G. Leofanti, M. Padovan, G. Busca, J. Catal. 191 (2000) 354–363.
[68] B.H. Aristizábal, C.M. de Correa, A.I. Serykh, C.E. Hetrick, M.D. Amiridis, Micro. Mesoporous Mater. 112 (2008) 432–440.
[69] G. Busca, Catal. Today 27 (1996) 457–496.
[70] V.V. Kaichev, V.I. Bukhtiyarov, M. Hävecker, A. Knop-Gercke, R.W. Mayer, R. Schlögl, Kinet. Catal. 44 (2003) 432–440.